Polyvinylpyrrolidone modified graphene oxide as a modifier for thin film composite forward osmosis membranes

Xing Wu[1, 2], R Field[3], Jun Jie Wu[4], Kaisong Zhang[1]*

1. *Key Laboratory of Urban Pollutant Conversion, Institute of Urban Environment, Chinese Academy of Sciences, Xiamen, 361021, China*
2. *University of Chinese Academy of Sciences, Beijing, 100049, China*
3. *Department of Engineering Science, University of Oxford, Oxford, OX1 3PJ, UK.*
4. *School of Engineering and Computing Sciences, Durham University, Durham, DH1 3LE, UK*

** Corresponding author: K. S. Zhang, Tel/ Fax: +86 592 6190782. Email: kszhang@iue.ac.cn*

Abstract

Polyvinylpyrrolidone (PVP) modified graphene oxide (GO), hereinafter referred to as PVP-GO, was synthesized as a novel modifier to fabricate thin film nanocomposite forward osmosis membranes. The results indicated that by coating PVP on the surface of GO nanosheets, the dispersibility of GO was increased and the aggregation of GO was reduced. Compared with the pristine and GO modified FO membranes, the PVP-GO modified membranes enhanced the desalination performance giving both a higher water flux and lower reverse solute flux. When using 2 $mol \cdot L^{-1}$ of NaCl as the draw solution and 10 $mmol \cdot L^{-1}$ NaCl as the feed solution, the water flux of the FO membrane modified with 0.0175 wt.% of PVP-GO reached 33.2 LMH in the ALDS mode (the active layer facing the draw solution), which was 3.3 times higher compared with the water flux of the pristine FO membranes. Improved desalination performances of PVP-GO modified FO membranes were attributed to the better dispersibility of the PVP-GO nanosheets and increased surface hydrophilicity of the modified FO membranes. This study indicated that PVP-GO is an effective modifier to enhance the performance of FO membranes.

Keywords: Graphene oxide; Forward osmosis; Thin film nanocomposite membrane; Desalination

1. Introduction

Membrane-based techniques such as ultrafiltration (UF), nanofiltration (NF), and reverse osmosis (RO) are commonly applied to manage waste water treatment and seawater desalination [1-3]. Forward osmosis (FO) is a process that uses an osmotic pressure gradient as the driving force to extract pure water out of saline water. In the water treatment area FO has been seen as having potential due to prospective lower energy costs and positive effects with regard to the mitigation of membrane fouling compared to traditional pressure-driven membranes [4-8] but reservations about its industrial potential have been expressed [9].The challenges include the need for thin film composite FO membranes (TFC-FO) to have higher water fluxes, reduced reverse flux of salt and the need to lessen internal concentration polarization (ICP) [10-12].

Many studies have been performed to improve TFC membrane performance through membrane modifications. One of the most prevalent strategies is to embed nanoparticles into membranes. It was reported that materials such as silver, TiO_2, carbon nanotubes (CNTs), and ZnO could be blended into membranes to alter certain membrane properties including porosity, roughness and hydrophilicity, which enhanced membrane performances [13-16]. Another strategy is to modify the surface of the membranes either to improve membrane permeability/rejection or to reduce fouling. It was reported that by adding silicon dioxide into aqueous solutions during the interfacial polymerization process, the water flux of the FO membrane was increased and the reverse solute flux was reduced [17]. Embedded silver nanoparticles into the surface of membranes has been found to reduce the membrane fouling since silver nanoparticles interacted with bacteria directly [18-21].

Recently carbon-based nanomaterials have attracted attention as a novel membrane modifier. Among these nanomaterials, graphene and graphene oxide (GO) have become buzzwords in recent years due to advantages such as large surface area, great compatibility, prominent electron transport and great mechanical properties [22]. Enhancements of both water flux and sodium sulfate rejection were reported when GO was added into polysulfone (PSf) ultrafiltration (UF) membranes [23]. Ionita and co-workers found that GO modified PSf-UF membranes showed improved thermal and

mechanical performances [24]. However, the required added amount of nanoparticles was rather large with over 0.25 wt.% [24]. Previous reports associated with RO membrane modification have focused on adding a relatively small amount of GO directly into the aqueous phase solution during the interfacial polymerization process. Whilst there were observed improvements in membrane performances such as water flux, salt rejection and antifouling, the aggregation of GO could not be ignored at a relatively high concentration [25, 26]. Ali and co-workers reported that the separation performance of TFC membranes was reduced when the concentration of GO was higher than 0.015 wt.% of aqueous phase solution [27]. Therefore, it is important to have a more efficient strategy for proper dispersion of graphenes and grahene oxide.

Polyvinylpyrrolidone (PVP), a pore-forming macromolecule with non-ionic and non-toxic properties, is a common reagent to control the microstructure of UF membranes [28], it is also a hydrophilic modifier to reduce membrane fouling [29]. Moreover, previous studies have confirmed that PVP is an excellent surface modifier in improving and stabilizing the dispersion of nanoparticles [30]. It was reported that graphenes could be detached from graphites by using PVP in the aqueous phase under sonication, which enabled polymer-coated single layers of graphenes to disperse stably in the aqueous phase [31]. Besides these advantages, however, PVP is easily washed away and difficult to retain inside membranes [32]. An appropriate solution should be provided to reduce the run off of PVP if using it for membrane surface modification.

To this end, a novel material, PVP-GO was prepared by coating PVP with graphene oxide nanoparticles (PVP-GO), which could not only increase the dispersion of GO but also reduce the run off of PVP at the same time. In addition, the feasibility of PVP-GO as a membrane modifier was investigated. PVP-GO modified FO membranes were characterized and their desalination performance investigated and compared with that of GO modified FO membranes. Moreover, the optimal loading of PVP-GO on the FO membranes was also investigated in this work. To the best of our knowledge, this is the first time that the feasibility of PVP-GO to modify the surface of FO membranes has been investigated.

2. Experimental

2.1. Materials

Polysulfone (PSf, Solvay P3500) was purchased from BASF Co., Ltd. (China). 1-methyl-2-pyrrolidinone (NMP, ≥ 99%) was bought from Sinopharm Chemical Reagent Co., Ltd. (China). Trimesoyl chloride (TMC, 98%) and m-phenylenediamine (MPD) were purchased from Aladdin (China). n-hexane (99%, Sinopharm Chemical Reagent Co., Ltd., China) was applied as the solvent of TMC. Graphene oxide (GO) (Aladdin, China) contains 30-40% oxygen-containing functional groups and a few layers of graphene oxide, in a thickness ranging from 0.55 to 1.2 nm. The TEM image of graphene oxide is shown in Fig. S1 in the Supporting Information. Polyvinylpyrrohdone (PVP K30, Sigma-Aldrich, China) and L-ascorbic acid (L-AA, 99%, Alfa Aesar, China) were used for graphene oxide modification. In addition, sodium chloride (NaCl) from Sinopharm Chemical Reagent Co., Ltd. (China) was used for membrane performance testing.

2.2. Preparation of PVP-GO nanoparticles

The PVP-GO was prepared by a synthesis method given in previous reports [25, 33]. Fig. 1 shows the schematic diagram of PVP-GO preparation. In this experiment, 250 mg of GO was added into 100 ml of deionized water and sonicated for 30 min to achieve the uniform dispersion. Following that, 25 mg of PVP and 50 mg of L-AA were added into the homogeneous GO dispersion at the same time. Initially the mixture was stirred for 10 min at room temperature and then for 4 h in a 80 °C water bath. Later, the suspension was centrifuged at 12,000 rpm for 15 min and washed with deionized water to remove excess PVP and L-AA. Finally, the product was re-dispersed into 100 ml deionized water for future use. For comparison, the homogeneous 25 $mg \cdot L^{-1}$ GO dispersion was stirred under room temperature for 4 h and 10 min without the addition of PVP and L-AA. Similarly, the GO dispersion was centrifuged and re-dispersed into 100 ml deionized water.

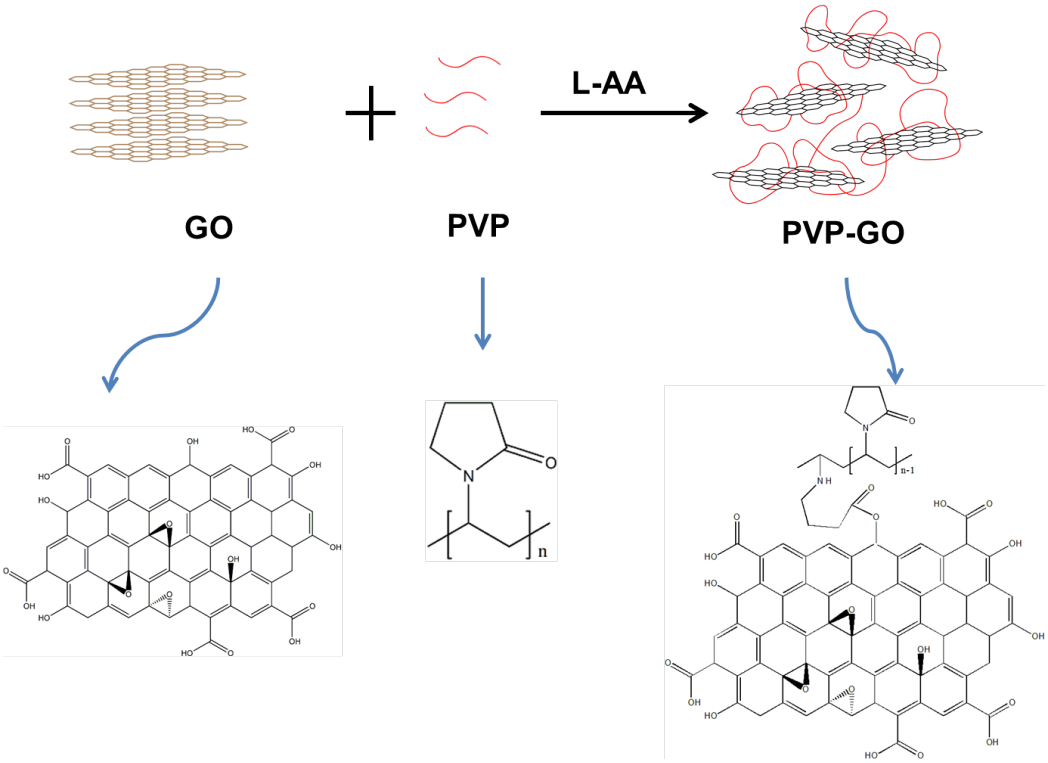

Fig. 1. Schematic diagram of the preparation of PVP-GO.

2.3. Preparation of GO and PVP-GO modified FO membranes

The PSf substrate membrane was prepared through a typical phase inversion technique. Generally, 0.5 wt.% of PVP and 17.5 wt.% of PSf were dissolved into 82 wt.% NMP. The casting solution was spread on a clean glass plate at a knife height of 175 μm. The permeate flux of pure water of this substrate membrane was approximately 367 LMH under a pressure of 0.1 MPa, tested by a dead-end filtration testing system. Moreover, the rejection of 1 $g \cdot L^{-1}$ of bovine serum albumin (BSA) was 99.4%.

The prepared GO and the PVP-GO solution were diluted into the specific concentrations listed in Table 1. After that, 2.0 wt.% MPD was added into solutions containing different amounts of GO and PVP-GO, respectively. Through interfacial polymerization, the dense active polyamide (PA) layer of the FO membrane was prepared on the substrate membrane. Firstly, 2.0 wt.% MPD aqueous solution containing nanoparticles were poured onto the surface of the substrate membrane for 2 min. Excess MPD aqueous solution was removed by a rubber roller. After that, 0.1 wt.% TMC

dissolved in n-hexane was poured onto the surface of the membrane. After 1 min, the TMC solution was drained off. Later, the membrane was stored in an oven under 60 °C for 8 min. Finally, the membrane was stored in a deionized water bath for future use. According to the amount of GO in MPD solution, the membranes were named as GO-FO-1, GO-FO-2, GO-FO-3, GO-FO-4, GO-FO-5 and GO-FO-6, while PVP-GO modified FO membranes were labeled as PGO-FO-1, PGO-FO-2, PGO-FO-3, PGO-FO-4, PGO-FO-5 and PGO-FO-6.

Table 1. The concentration of nanoparticles in MPD solutions for interfacial polymerization.

Membrane	GO (wt.%)	Membrane	PVP-GO (wt.%)
TFC-FO	0		
GO-FO-1	0.0075	PGO-FO-1	0.0075
GO-FO-2	0.0100	PGO-FO-2	0.0100
GO-FO-3	0.0125	PGO-FO-3	0.0125
GO-FO-4	0.0150	PGO-FO-4	0.0150
GO-FO-5	0.0175	PGO-FO-5	0.0175
GO-FO-6	0.0200	PGO-FO-6	0.0200

2.4. Characterization of GO and PVP-GO nanoparticles

Ultraviolet-visible (UV-vis) spectra of GO and PVP-GO solutions were measured using a Cary-50 UV-vis spectrometer (Varian, USA). Attenuated total reflectance-infrared spectroscopy (ATR-FTIR, Nicolet iS10, Thermo Fisher Scientific, USA) was used to estimate the functional groups of nanoparticles. Additionally, Raman scattering spectra of GO and PVP-GO were collected by a LabRAM Aramis (HORIBA JobinYvon) confocal micro-Raman system. For obtaining Raman spectra, one drop of GO and PVP-GO solution was placed onto clean silicon wafers as the SERS substrate, respectively. After drying under room temperature, the Raman signals of GO and PVP-GO molecules were detected. Zeta potential of GO and PVP-GO solution were analysed by a ZetaPALS Zeta Potential Analyzer.

2.5. Characterization of FO membranes

In order to estimate the functional groups in the membrane surface, infrared spectra of membranes were obtained by ATR-FTIR. Before investigation, membrane samples were kept at room temperature for 24 h to dry. Additionally, in order to investigate the hydrophilicity of membranes, a sessile drop analysis system (DSA100, KRUSS, Germany) was applied to measure the contact angle of the membranes. The contact angles were tested immediately after placing a drop of deionized water on the surface of membranes. Prior to testing, every membrane sample was dried at room temperature for 24 h. Additionally, a field emission scanning electron microscope (FESEM, HITACHI S-4800, Japan) system was in place to observe the surface morphology of FO membranes. Before testing, all samples were kept in an oven for 48 h at 80 °C. Membrane surface roughness was analyzed by atomic force microscopy (AFM) (Aglient, USA) used in a peak force tapping mode in air.

2.6. Evaluation of desalination performance of FO membranes

All membranes were tested in a forward osmosis test system, which has been described previously [16, 34], in both the ALFS mode (the active layer facing the feed solution) and the ALDS mode (the active layer facing the draw solution) under room temperature. The total active membrane area was 33.8 cm^2, the draw solutions were 2 $mol \cdot L^{-1}$ NaCl and 0.5 $mol \cdot L^{-1}$ NaCl solution, respectively, while 10 $mmol \cdot L^{-1}$ NaCl was used as the feed solution. Both the draw solutions and the feed solutions were maintained at a cross-flow rate of 20 $L \cdot h^{-1}$. The weight change of the draw solutions and the conductivity change of the feed solution were measured by a digital weight balance and a conductivity meter, respectively. After 20 min of the FO system becoming stable, the water flux (J_w) and the reverse solute flux (J_s) were recorded. Both J_w and J_s were examined every 15 min over 5 times to calculate the average value. The following equations were applied for the calculation of water flux and reverse solute flux, respectively.

$$J_w = \frac{\Delta V}{\Delta t \cdot A_m} \tag{1}$$

$$J_s = \frac{\Delta(C_t V_t)}{\Delta t \cdot A_m} \quad (2)$$

where ΔV is the volume of permeated water (L), A_m is the membrane area (m^2), and Δt is the permeation time (h), C_t is the concentration of NaCl at the end of permeation time, V_t is the volume of permeated water at the end of permeation time (L).

3. Results and discussion

3.1. Characterization of GO and PVP-GO nanosheets

Fig. 2a shows pictures of GO and PVP-GO aqueous dispersions immediately and two weeks after being prepared. It was observed that there was no obvious precipitation of either GO or PVP-GO. Fig. 2b illustrates the UV-vis spectra result of GO, PVP and PVP-GO. Some typical peaks could be observed in GO nanosheets. The peak at 230 nm is associated with the π-π* transitions caused by the C-C bonds of the aromatic skeleton, while a shoulder peak at 300 nm resulted from the π-π* transitions caused by the C-O bonds of carboxylic acid [25, 33, 35]. Compared with GO, PVP-GO showed an obvious peak at 197 nm which is the typical peak of PVP, indicating that PVP was successfully coated on the surface of GO. Another difference between the spectra of PVP-GO and GO was that the absorption peak which was at 230 nm in GO shifted to at 270 nm in PVP-GO, while the intensity of the shoulder peak at 300 nm decreased, which showed that GO was reduced [35, 36]. In addition, the reduction of GO was the reason for color differences between GO and PVP-GO aqueous dispersions.

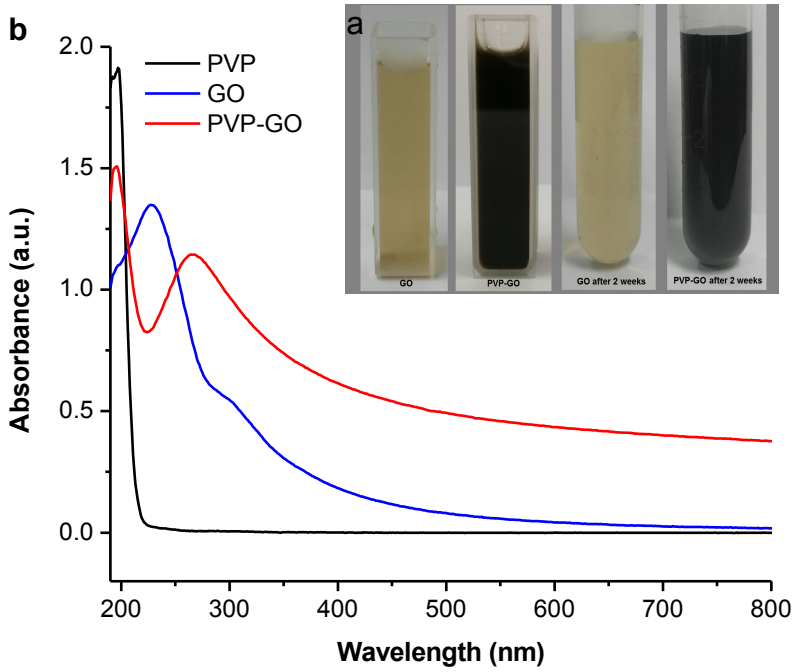

Fig. 2. (a) Photographs of aqueous dispersions of GO and PVP-GO taken immediately after preparation and two weeks later, (b) UV-vis spectra of aqueous dispersions of PVP, GO and PVP-GO.

Fig. 3a shows the ATR-FTIR spectra of GO and PVP-GO. It could be observed that there was a peak at 1726 cm^{-1} in the spectra of GO due to the oxygen-containing groups on the surface of the GO [37]. Nevertheless, the peak disappeared in the spectra of PVP-GO, indicating that some oxygen-containing groups on the GO surface were removed, and certain chemical bonds were built up between PVP molecules and some functional groups on the surface of GO sheets [37]. This change of PVP-GO indicated that GO was reduced by L-AA during the process of PVP-GO preparation. It was reported that at the beginning stage of PVP-GO synthesis, some *tert*-amide groups in PVP are protonated because of L-AA. After that, these active *tert*-amide groups reacted with the epoxide or the hydroxyl groups surrounding the surface of GO before the functional groups were reduced by L-AA (Fig. 1) [37]. The reduction of GO was also confirmed through evidence of Raman scattering (Fig. 3b). The spectra of GO indicated that there were two characteristic peaks at 1338 cm^{-1} and 1595 cm^{-1}, which represented the D band and the G band, respectively [38]. After the GO was coated with PVP, the intensity ratios of the D

and the G band of PVP-GO increased from 0.97 to 1.29, confirming that the GO was reduced during the preparation of PVP-GO [39]. However, the peak at around 3443 cm^{-1} of the ATR-FTIR spectra of PVP-GO suggested that there were still hydroxyl groups on the surface of the PVP-GO [40]. The zeta potential (ZP) of GO and PVP-GO aqueous solutions were tested. Zeta potential reflects how much charged particles repel each other in dispersion. Thus, a high absolute value of zeta potential generally indicates that the level of aggregation is low and the dispersion is stable [38, 41-43]. Results showed that the zeta potential was -25.0 mV for GO and -35.1 mV for PVP-GO, which revealed a higher stability of PVP-GO aqueous solution than the GO aqueous solution.

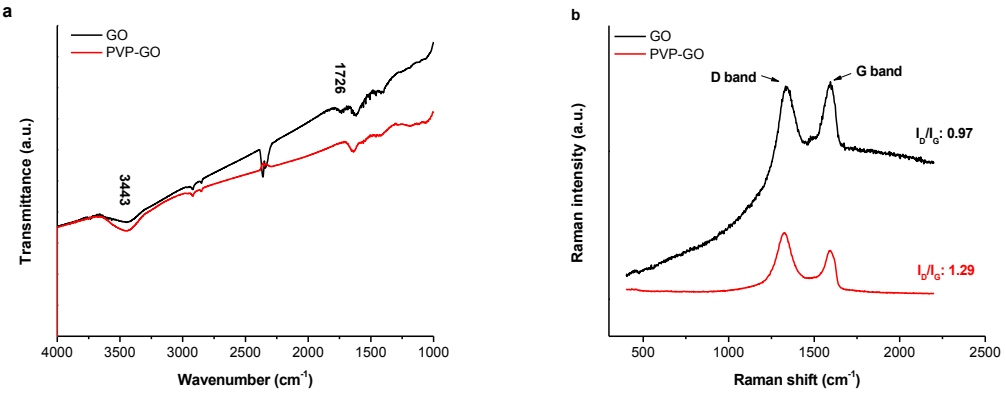

Fig. 3. (a) ATR-FTIR spectra of GO and PVP-GO nanosheets, (b) Raman spectra of GO and PVP-GO nanosheets.

3.2. Characterization of FO membranes

ATR-FTIR spectra of the pristine TFC-FO membrane and membranes modified by 0.015 wt.% of GO (GO-FO-4) and PVP-GO (PGO-FO-4) were examined (Fig. 4). It was observed that all FO membranes showed some typical peaks of polyamide membranes prepared by interfacial polymerization of MPD and TMC. The peaks at 1322, 1295 and 1146 cm^{-1} were due to the stretching vibration of the asymmetric sulfur dioxide while the peak at 1411 cm^{-1} was attributed to C-H symmetric deformation vibration of $-C(CH_3)_2$ [44]. Evidence of the existence of GO and PVP-GO on the surface of modified TFC-FO membranes was shown in a new broad peak around 3443 cm^{-1}, which belonged to the hydroxyl stretching vibration of GO and PVP-GO [40]. Due to the small amount of nanoparticles, this peak was not obvious. Compared with the pristine TFC-FO

membranes, GO and PVP-GO modified membranes showed increasing transmittance intensity at 1726 cm^{-1}. This is due to the oxygen-containing groups on the GO and PVP-GO surface which is in line with the results of ATR-FTIR measurements on GO and PVP-GO. These results together confirmed the presence of GO and PVP-GO nanosheets on the surfaces of FO membranes after interfacial polymerization.

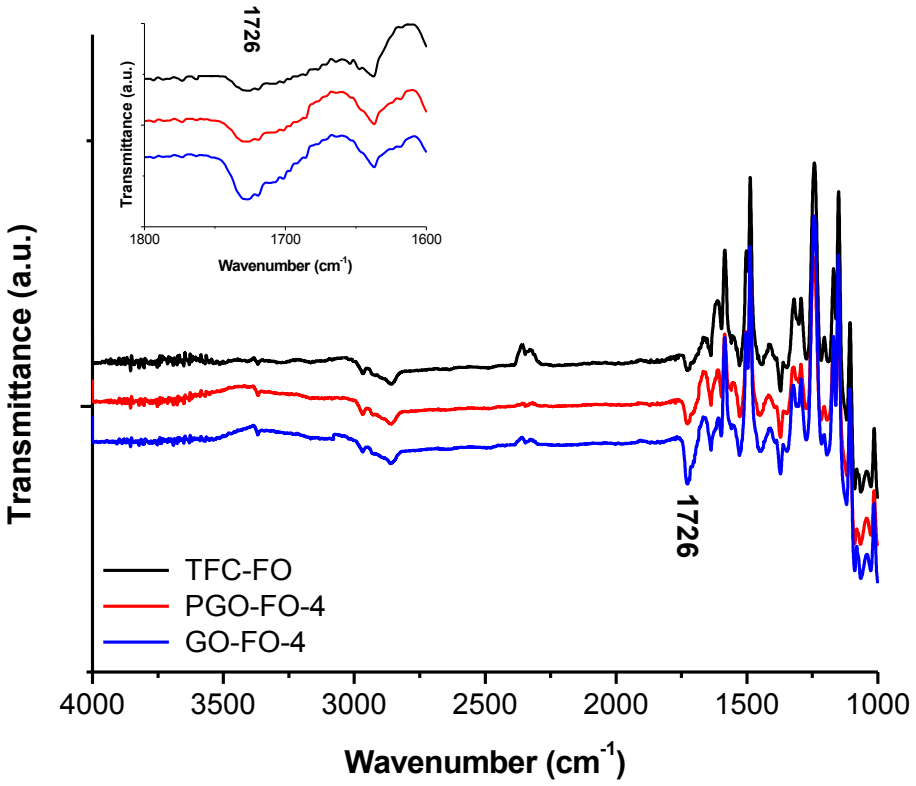

Fig. 4. ATR-FTIR spectra of TFC-FO, GO-FO-4 and PGO-FO-4 membranes.

Fig. 5 shows the water contact angles of FO membranes modified by different amounts of GO or PVP-GO. It was observed that the contact angles decreased with the increasing concentrations of GO or PVP-GO. This was due to the hydroxyl functional groups around GO and PVP-GO, which were confirmed by the ATR-FTIR results shown in Fig. 3a and Fig. 4, respectively. Moreover, compared with the contact angles of GO-FO membranes, PGO-FO membranes showed slightly lower contact angles at the same concentration of nanoparticles. This indicated that the hydrophilic PVP also increases the hydrophilicity of membrane surface, which was in line with other research [32].

Therefore, it could be expected that PVP-GO modified FO membranes might demonstrate a higher water flux.

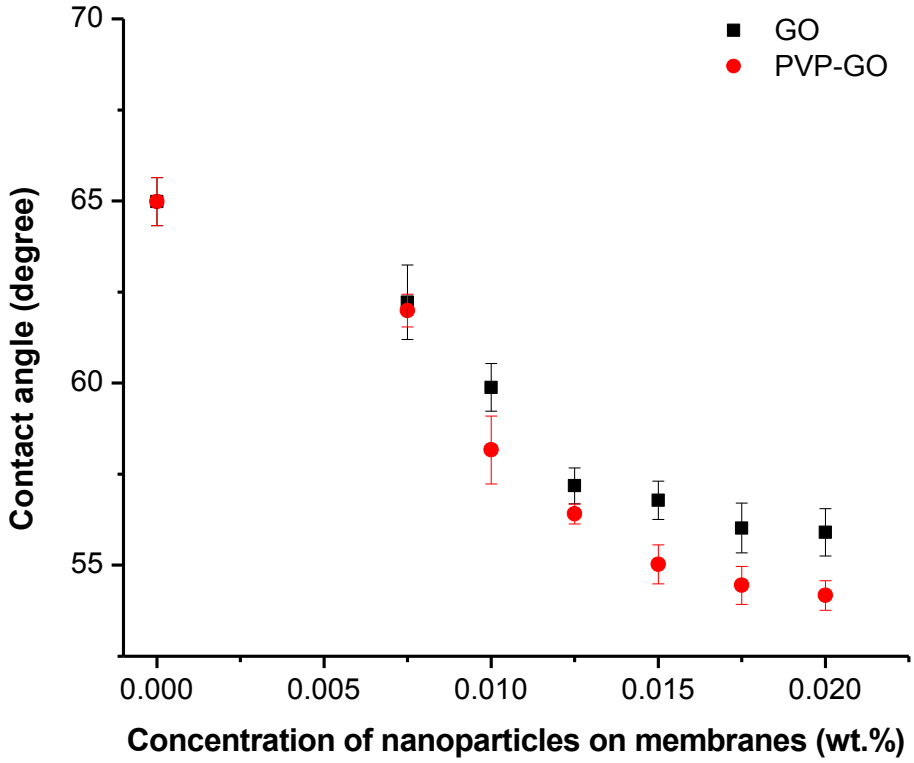

Fig. 5. Contact angles of membranes with different concentrations of GO and PVP-GO.

Fig. 6 shows the FESEM images of the surface of thin film nanocomposite forward osmosis (TFN-FO) membranes and of a TFC-FO membrane. The typical "ridge and valley" structures formed by the interfacial polymerization process were found in all membranes [45]. It could be observed that the pristine TFC-FO membrane had a dense cross-linking network that covered the globular structure and left only a few globules exposed. While GO concentrations increased, more globules were observed on the surface of membranes (Fig. 6b and 6d). There were some regions on the GO-FO-6 membrane that were smooth and without any cover of globules or crosslinking networks. A computer software "Image J" was used to measure the percentage of smooth area on the membrane surfaces. Firstly, the area of smooth regions (in Fig. 6d and Fig. 6e respectively) were highlighted and measured by the software. After that, the area of the

smooth regions was divided by the total area of the SEM image to illustrate the percentage of smooth area on membrane surfaces. Results indicated that the smooth area of GO-FO-6 occupied almost 37.9% of the membrane surface in Fig. 6d, while PGO-FO-6 had a smooth area of 17.3%. The effect of GO and PVP-GO on surface roughness was also investigated by analyzing the surface topology using AFM. Fig. 7 shows the three dimensional AFM images of the top surface of the pristine TFC-FO, GO-FO-5, PGO-FO-5, GO-FO-6 and PGO-FO-6 membranes with a scan size of 5 μm × 5 μm. Table 2 shows the average arithmetic roughness (Ra), root mean square roughness (Rq) and irregularities (Rz) of these membranes. Compared with the pristine TFC-FO membrane, GO modified FO membranes and PVP-GO modified FO membranes showed smoother surfaces. Moreover, when FO membranes were modified by the same concentration of nanosheets, PVP modified FO membranes showed less reduction of roughness parameters than GO modified FO membranes. The reason for these smooth areas and the reduction of roughness was connected to the interaction of aggregated GO during the interfacial polymerization process. The formation of ridge structures depended on the diffusion of MPD into the organic side during the interfacial polymerization process. When GO nanosheets were embedded into the MPD solution, they would transversely adhere to each other during the interfacial polymerization process. As a result, the aggregation of GO nanosheets interfered with the diffusion of MPD and hindered the development of the ridge structures [46-48]. Compared with GO modified FO membranes, the reduced smooth area in PVP modified FO membranes was potentially due to the better dispersibility of PVP-GO than GO, and a reduced amount of aggregation. Fig. 8 exhibits the cross-sections of the TFC-FO membrane and PGO-FO-5. Using "Image J", the thickness of the PA layer was measured by comparing the width of the PA layer and the scale in SEM images. 20 locations were selected in each SEM image to calculate the average thickness of the PA layer. It could be observed that the thickness of the polyamide layer of PGO-FO-5 membrane was 154 nm, which was less than the 253 nm of the TFC-FO membranes. This result was in line with other research and was potentially caused by the interference of GO with the interfacial polymerization process which, as noted above, hindered the formation of ridge structures on the surface of TFC membranes [46, 49].

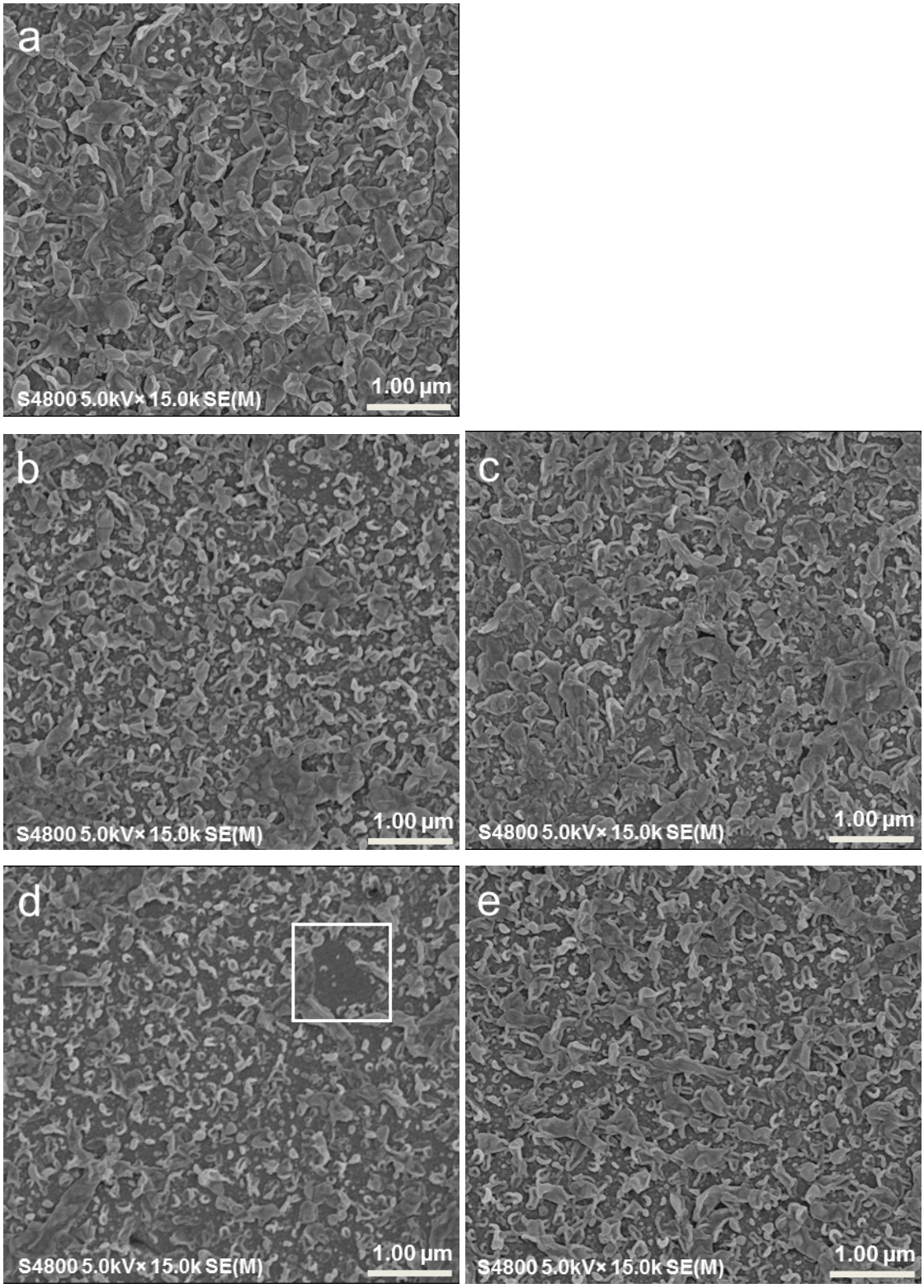

Fig. 6. SEM images of surfaces of (a) TFC-FO, (b) GO-FO-5, (c) PGO-FO-5, (d) GO-FO-6, and (e) PGO –FO-6 membranes.

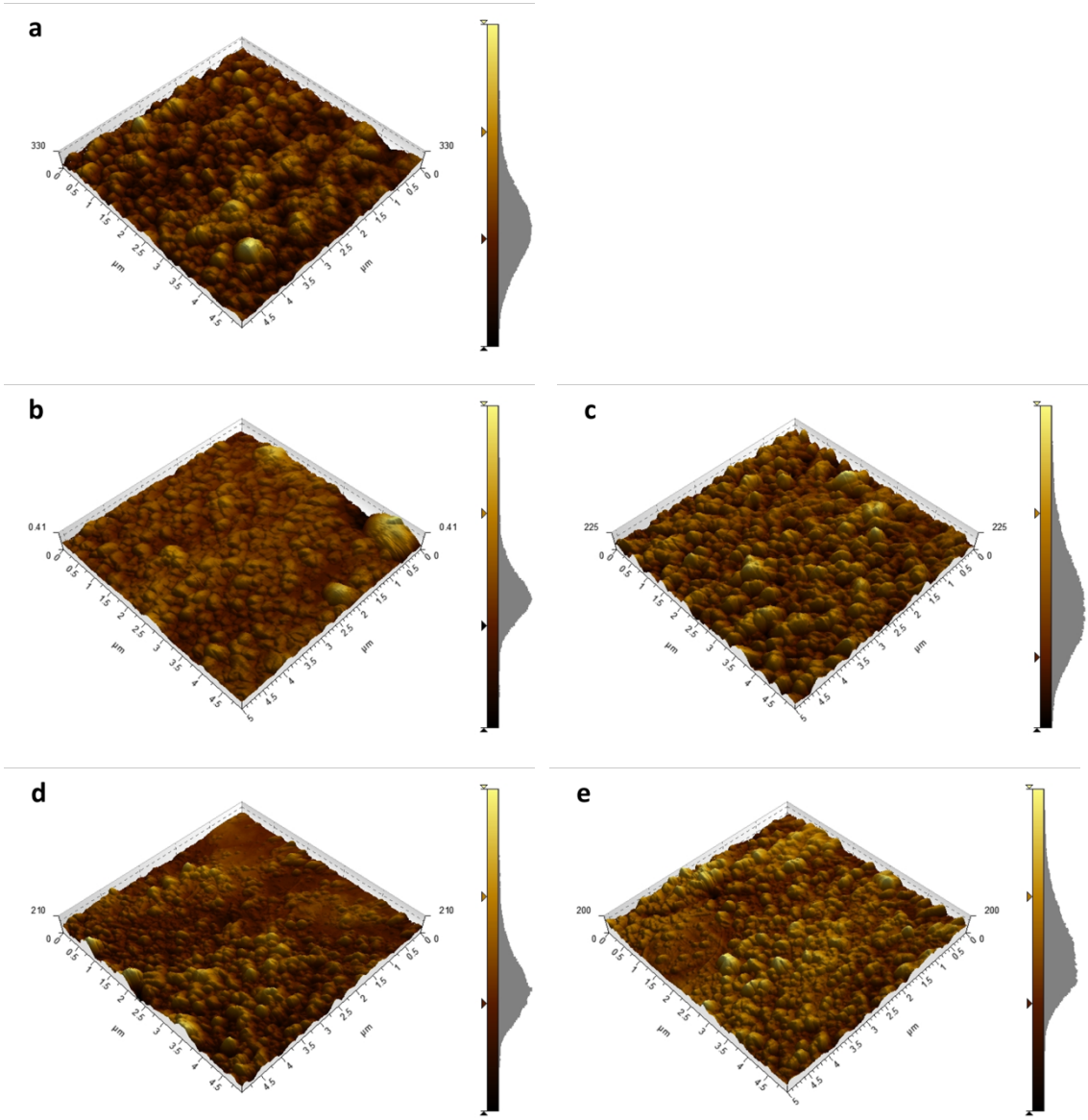

Fig. 7. Surface AFM 3D images of (a) TFC-FO, (b) GO-FO-5, (c) PGO-FO-5, (d) GO-FO-6, and (e) PGO –FO-6 membranes.

Table 2. Roughness parameters of TFC-FO, GO-FO-5, PGO-FO-5, GO-FO-6 and PGO-FO-6 membranes.

Membrane	Ra (nm)	Rq (nm)	Rz (nm)
TFC-FO	19.9 ± 2.0	24.8 ± 2.7	124 ± 5.0
GO-FO-5	14.5 ± 0.4	17.7 ± 0.5	87.3 ± 0.9
PGO-FO-5	18.1 ± 1.9	21.8 ± 1.3	97.3 ± 3.7
GO-FO-6	11.9 ± 0.3	14.8 ± 0.6	70.6 ± 3.3

PGO-FO-6	13.8 ± 0.2	17.4 ± 0.8	82.5 ± 3.9

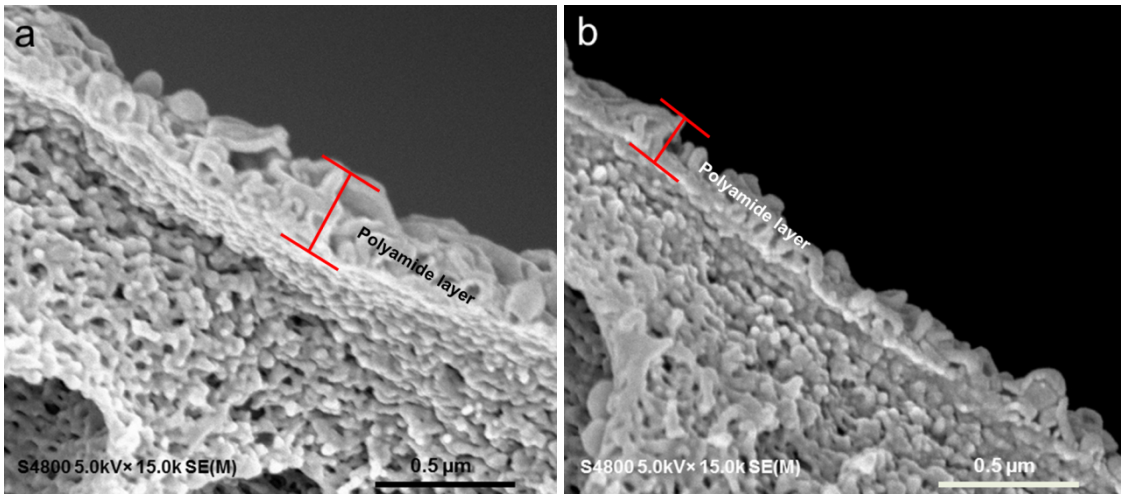

Fig. 8. SEM images of cross sections of (a) TFC-FO membrane, and (b) PGO-FO-5 membrane.

3.3. Desalination performances of FO membranes

Fig. 9 and 10 show the water fluxes of the FO membranes modified by different concentrations of GO and PVP-GO in the ALFS mode and the ALDS mode with different concentrations of draw solutions. It could be observed that the water fluxes of both GO-FO and PGO-FO membranes showed similar tendencies; with increasing concentrations of modifers the water fluxes initially increased and reached optimal values typically being at 0.015 wt.% for GO and 0.0175 wt.% for PVP-GO. Compared with the TFC-FO membrane, all TFN-FO membranes showed enhancements in water fluxes, which indicated both GO and PVP-GO were good modifiers to improve the water flux for FO membranes. The optimal water flux of GO-FO membranes was achieved when 0.015 wt.% of GO was added into the MPD solution, with the water flux increasing 62.2% (from 6.66 LMH to 10.80 LMH) in the ALFS mode and 58.4% (from 10.19 to 16.4 LMH) in the ALDS mode when using 2 mol·L^{-1} NaCl solution as the draw solution. Under the same operating conditions, the PGO-FO-5 membrane showed the highest water flux which increased 113% in the ALFS mode and 226% in the ALDS mode. This enhancement of water fluxes was due to the improvement of the hydrophilicity introduced by the hydrophilic functional groups around the surface of GO and PVP-GO.

The hydrophilic surface improved the adsorption of water molecules on the membrane surface and possibly increased the diffusion rate of water molecules passing through the modified membranes [44, 50]. Moreover, the thinner polyamide layer of the TFN-FO membranes was also was a critical factor in improving the water fluxes.

Compared with the water fluxes of GO-FO membranes, the water fluxes of all the PVP-GO modified membranes were higher when modified by the same concentration of GO. This was potentially associated with enhancements in both the hydrophilicity and the dispersibility of PVP-GO. It has been reported that PVP tends to attract water molecules [37, 51] which would enhance the relative hydrophilicity of PVP-GO membranes. However, when the concentration of GO and PVP-GO reached 0.0175 wt.% and 0.02 wt.%, respectively, the water fluxes had passed their optima. This could be due to aggregation of nanoparticles at higher concentrations. As shown in SEM and AFM images, an enlarged smooth area could be observed when the concentration of GO increased to 0.02 wt.%, (Fig. 6d and 7d). The smooth region on the surface of the GO-FO-6 membrane reduced the surface roughness and resulted in a smaller active area of the PA layer, consequently reducing the water flux. Compared with the GO-FO-6 membrane, the PGO-FO-6 membrane had fewer smooth regions. This is potentially due to the PVP-GO being better dispersed.

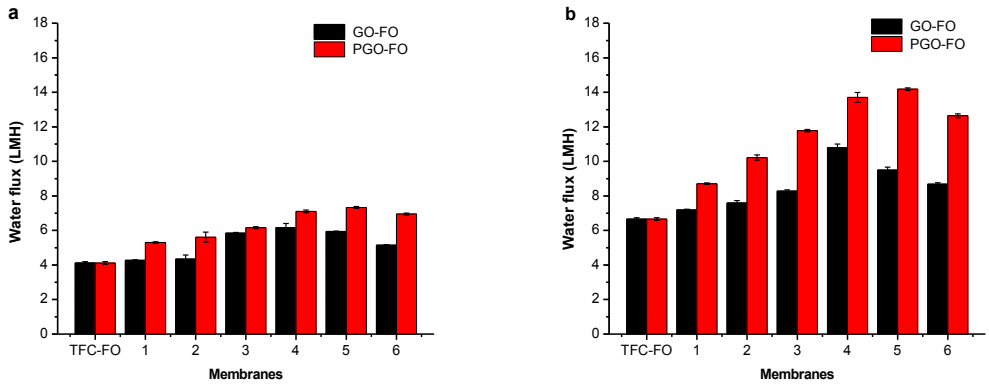

Fig. 9. Water flux of FO membranes in the ALFS mode (a) 0.5 mol·L^{-1} of draw solution, (b) 2.0 mol·L^{-1} of draw solution. 10 mmol·L^{-1} NaCl as the feed solution and cross-flow rate was 20 L·h^{-1}.

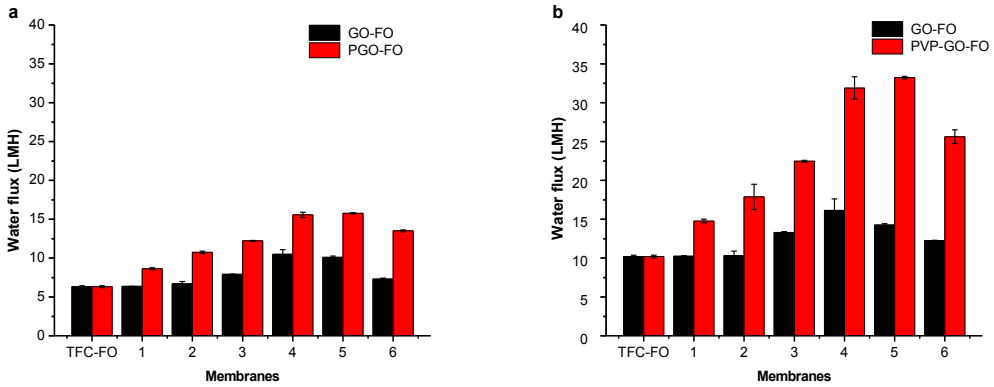

Fig. 10. Water flux of FO membranes in the ALDS mode (a) 0.5 mol·L^{-1} of draw solution, (b) 2.0 mol·L^{-1} of draw solution. 10 mmol·L^{-1} NaCl as the feed solution.

The ratio of reverse solute flux and water flux is another critical factor with which to evaluate the performance of FO membranes [52]. Higher ratios indicate that there is relatively more salt moving from the draw solution to the feed solution and the membrane has looser dynamic pore structure [53]. Fig. 11 shows the values of J_S/J_W of FO membranes modified by different amounts of GO and PVP-GO. Generally, the trend of J_S/J_W for both the GO-FO and the PVP-GO-FO membranes reduced and then increased along with increasing concentrations of nanosheets. Under all four operating conditions, it could be observed that GO-FO-4 and GO-FO-5 showed the lowest values of J_S/J_W. Compared with values of J_S/J_W of the GO-FO membranes, more obvious reductions could be observed on J_S/J_W of PGO-FO membranes. Specially, when the concentration of PVP-GO was 0.015 or 0.0175 wt.%, the J_S/J_W of PVP-GO-FO membrane was at a minimum. Not unexpectedly the concentrations which maximised water flux also minimised J_S/J_W. Thus when the concentration of GO was larger than 0.015 wt.% and when the concentration of PVP-GO was larger than 0.0175 wt.%, the values of J_S/J_W of modified membranes increased. This could be caused by the aggregation of nanoparticles.

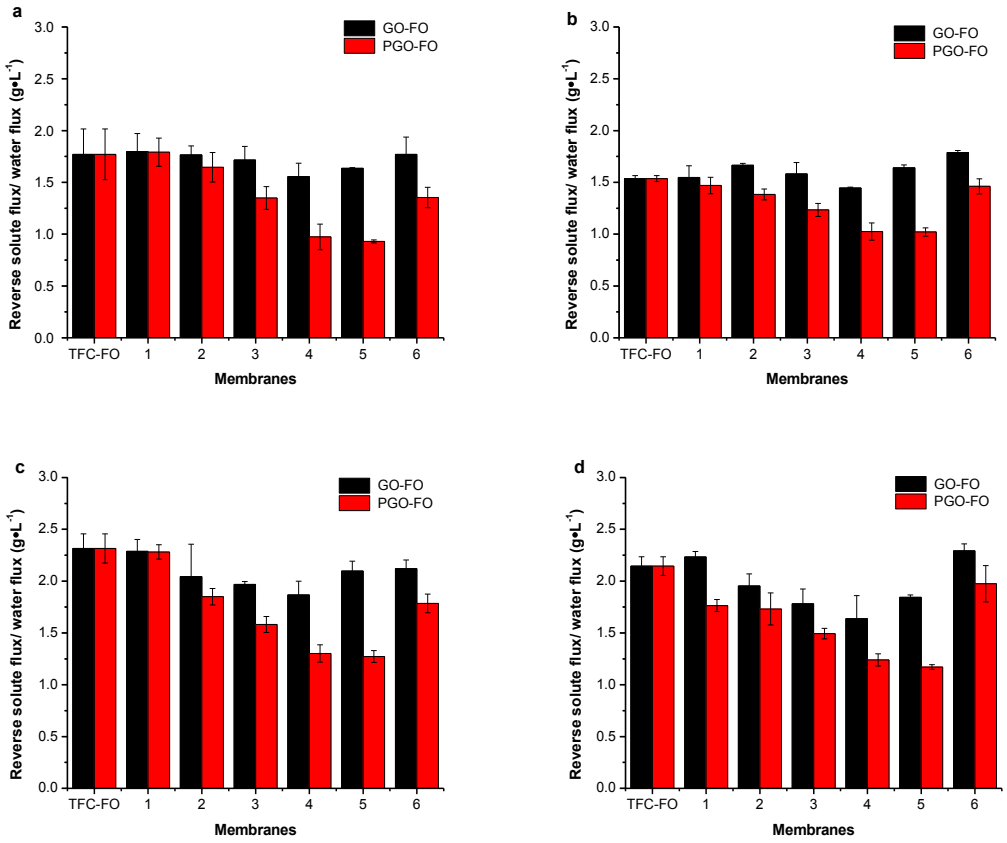

Fig. 11. Ratio of reverse solute flux and water flux of modified FO membranes with different amounts of GO and PVP-GO in (a) ALFS mode with 0.5 mol·L^{-1} of draw solution, (b) ALFS mode with 2.0 mol·L^{-1} of draw solution, (c) ALDS mode with 0.5 mol·L^{-1} of draw solution, and (d) ALDS mode with 2.0 mol·L^{-1} of draw solution. 10 mmol·L^{-1} NaCl as the feed solution.

4. Conclusion

In this study, PVP coated GO was prepared and the effects of PVP-GO on the desalination performances of TFN-FO membranes were investigated. Compared with GO nanosheets, results for PVP-GO displayed better dispersion and a lower tendency of aggregation. In addition, PVP-GO modified FO membranes exhibited excellent desalination performance, including improved hydrophilicity, enhanced water flux and reduced reverse solute flux compared to the pristine and GO modified FO membranes. Moreover, the negative influences of the aggregation of nanoparticles on the performance of membranes were reduced when PVP-GO was used in the replacement of the GO

modifier. The optimal loading of nanosheets on MPD was dependent on different types of nanoparticles. Among all of the modified TFN-FO membranes, the membrane that was modified with 0.0175 wt.% PVP-GO nanosheets showed the optimal desalination performance.

Acknowledgements

K.S.Z. and R.W.F. thank the Royal Academy of Engineering, UK for a research exchange under the China/India scheme and J.J.W. thanks the Royal Academy of Engineering for her Global Research Award. X.W. is grateful to Dr. Zongli Xie, Mr. Derrick Ng and Dr. Ruizhi Pang for their helpful suggestions. X.W. also appreciates Ms. Siqian Tu and Ms. Amanda Wareham for English editing. The authors gratefully acknowledge the financial support by Xiamen Municipal Bureau of Science and Technology (3502Z20131159) and Bureau of International Cooperation, CAS. The authors are also grateful to the reviewers for their helpful and insightful comments.

References

[1] A.W. Mohammad, Y. Teow, W. Ang, Y. Chung, D. Oatley-Radcliffe, N. Hilal, Nanofiltration membranes review: Recent advances and future prospects, Desalination, 356 (2015) 226-254.
[2] K. Katsoufidou, D. Sioutopoulos, S. Yiantsios, A. Karabelas, UF membrane fouling by mixtures of humic acids and sodium alginate: fouling mechanisms and reversibility, Desalination, 264 (2010) 220-227.
[3] K.P. Lee, T.C. Arnot, D. Mattia, A review of reverse osmosis membrane materials for desalination—development to date and future potential, J. Membr. Sci., 370 (2011) 1-22.
[4] Y. Sun, L. Xue, Y. Zhang, X. Zhao, Y. Huang, X. Du, High flux polyamide thin film composite forward osmosis membranes prepared from porous substrates made of polysulfone and polyethersulfone blends, Desalination, 336 (2014) 72-79.
[5] T.-S. Chung, X. Li, R.C. Ong, Q. Ge, H. Wang, G. Han, Emerging forward osmosis (FO) technologies and challenges ahead for clean water and clean energy applications, Curr. Opin. Chem. Eng., 1 (2012) 246-257.
[6] S. Zhao, L. Zou, C.Y. Tang, D. Mulcahy, Recent developments in forward osmosis: Opportunities and challenges, J. Membr. Sci., 396 (2012) 1-21.

[7] E.M. Garcia-Castello, J.R. McCutcheon, Dewatering press liquor derived from orange production by forward osmosis, J. Membr. Sci., 372 (2011) 97-101.
[8] B.E. Logan, M. Elimelech, Membrane-based processes for sustainable power generation using water, Nature, 488 (2012) 313-319.
[9] R.W. Field, J.J. Wu, Mass transfer limitations in forward osmosis: Are some potential applications overhyped?, Desalination, 318 (2013) 118-124.
[10] K. Lutchmiah, A.R. Verliefde, K. Roest, L.C. Rietveld, E.R. Cornelissen, Forward osmosis for application in wastewater treatment: a review, Water Res., 58 (2014) 179-197.
[11] M. Qasim, N.A. Darwish, S. Sarp, N. Hilal, Water desalination by forward (direct) osmosis phenomenon: A comprehensive review, Desalination, 374 (2015) 47-69.
[12] Y. Huang, H. Jin, P. Yu, Y. Luo, Polyamide thin-film composite membrane based on nano-silica modified polysulfone microporous support layer for forward osmosis, Desalin. Water Treat., 57 (2016) 20177-20187.
[13] D. Li, Y. Yan, H. Wang, Recent advances in polymer and polymer composite membranes for reverse and forward osmosis processes, Prog. Polym. Sci., (2016).
[14] D. Perera, S. Nataraj, N. Thomson, A. Sepe, S. Hüttner, U. Steiner, H. Qiblawey, E. Sivaniah, Room-temperature development of thin film composite reverse osmosis membranes from cellulose acetate with antibacterial properties, J. Membr. Sci., 453 (2014) 212-220.
[15] D. Emadzadeh, W.J. Lau, T. Matsuura, N. Hilal, A.F. Ismail, The potential of thin film nanocomposite membrane in reducing organic fouling in forward osmosis process, Desalination, 348 (2014) 82-88.
[16] D. Emadzadeh, W.J. Lau, T. Matsuura, A.F. Ismail, M. Rahbari-Sisakht, Synthesis and characterization of thin film nanocomposite forward osmosis membrane with hydrophilic nanocomposite support to reduce internal concentration polarization, J. Membr. Sci., 449 (2014) 74-85.
[17] N. Niksefat, M. Jahanshahi, A. Rahimpour, The effect of SiO2 nanoparticles on morphology and performance of thin film composite membranes for forward osmosis application, Desalination, 343 (2014) 140-146.
[18] J. Yin, Y. Yang, Z. Hu, B. Deng, Attachment of silver nanoparticles (AgNPs) onto thin-film composite (TFC) membranes through covalent bonding to reduce membrane biofouling, J. Membr. Sci., 441 (2013) 73-82.
[19] M. Zhang, R.W. Field, K. Zhang, Biogenic silver nanocomposite polyethersulfone UF membranes with antifouling properties, J. Membr. Sci., 471 (2014) 274-284.
[20] S. Liu, F. Fang, J. Wu, K. Zhang, The anti-biofouling properties of thin-film composite nanofiltration membranes grafted with biogenic silver nanoparticles, Desalination, 375 (2015) 121-128.
[21] S. Liu, M. Zhang, F. Fang, L. Cui, J. Wu, R. Field, K. Zhang, Biogenic silver nanocomposite TFC nanofiltration membrane with antifouling properties, Desalin. Water Treat., 57 (2016) 10560-10571.
[22] M. Safarpour, A. Khataee, V. Vatanpour, Thin film nanocomposite reverse osmosis membrane modified by reduced graphene oxide/TiO2 with improved desalination performance, J. Membr. Sci., 489 (2015) 43-54.

[23] B.M. Ganesh, A.M. Isloor, A.F. Ismail, Enhanced hydrophilicity and salt rejection study of graphene oxide-polysulfone mixed matrix membrane, Desalination, 313 (2013) 199-207.
[24] M. Ionita, E. Vasile, L.E. Crica, S.I. Voicu, A.M. Pandele, S. Dinescu, L. Predoiu, B. Galateanu, A. Hermenean, M. Costache, Synthesis, characterization and in vitro studies of polysulfone/graphene oxide composite membranes, Compos. Part B. Eng., 72 (2015) 108-115.
[25] L. Wang, R. Yang, H. Wang, J. Li, L. Qu, P.d.B. Harrington, High-selective and sensitive voltammetric sensor for butylated hydroxyanisole based on AuNPs–PVP–graphene nanocomposites, Talanta, 138 (2015) 169-175.
[26] L. He, L.F. Dumée, C. Feng, L. Velleman, R. Reis, F. She, W. Gao, L. Kong, Promoted water transport across graphene oxide–poly (amide) thin film composite membranes and their antibacterial activity, Desalination, 365 (2015) 126-135.
[27] M.E. Ali, L. Wang, X. Wang, X. Feng, Thin film composite membranes embedded with graphene oxide for water desalination, Desalination, 386 (2016) 67-76.
[28] X. Chang, Z. Wang, S. Quan, Y. Xu, Z. Jiang, L. Shao, Exploring the synergetic effects of graphene oxide (GO) and polyvinylpyrrodione (PVP) on poly (vinylylidenefluoride)(PVDF) ultrafiltration membrane performance, Appl. Surf. Sci., 316 (2014) 537-548.
[29] A.M. Telford, M. James, L. Meagher, C. Neto, Thermally cross-linked PNVP films as antifouling coatings for biomedical applications, ACS Appl. Mater. Interfaces., 2 (2010) 2399-2408.
[30] C. Ong, W. Lau, P. Goh, B. Ng, A. Ismail, Preparation and characterization of PVDF–PVP–TiO2 composite hollow fiber membranes for oily wastewater treatment using submerged membrane system, Desalin. Water Treat., 53 (2015) 1213-1223.
[31] A.B. Bourlinos, V. Georgakilas, R. Zboril, T.A. Steriotis, A.K. Stubos, C. Trapalis, Aqueous-phase exfoliation of graphite in the presence of polyvinylpyrrolidone for the production of water-soluble graphenes, Solid State Commun., 149 (2009) 2172-2176.
[32] J. Wu, Z. Wang, W. Yan, Y. Wang, J. Wang, S. Wang, Improving the hydrophilicity and fouling resistance of RO membranes by surface immobilization of PVP based on a metal-polyphenol precursor layer, J. Membr. Sci., 496 (2015) 58-69.
[33] X. Zhi, H. Fang, C. Bao, G. Shen, J. Zhang, K. Wang, S. Guo, T. Wan, D. Cui, The immunotoxicity of graphene oxides and the effect of PVP-coating, Biomaterials, 34 (2013) 5254-5261.
[34] M.J. Park, S. Phuntsho, T. He, G.M. Nisola, L.D. Tijing, X.-M. Li, G. Chen, W.-J. Chung, H.K. Shon, Graphene oxide incorporated polysulfone substrate for the fabrication of flat-sheet thin-film composite forward osmosis membranes, J. Membr. Sci., 493 (2015) 496-507.
[35] Q. Wang, N. Plylahan, M.V. Shelke, R.R. Devarapalli, M. Li, P. Subramanian, T. Djenizian, R. Boukherroub, S. Szunerits, Nanodiamond particles/reduced graphene oxide composites as efficient supercapacitor electrodes, Carbon, 68 (2014) 175-184.
[36] D. Li, M.B. Mueller, S. Gilje, R.B. Kaner, G.G. Wallace, Processable aqueous dispersions of graphene nanosheets, Nat. Nanotechnol., 3 (2008) 101-105.
[37] J. Zhang, G. Shen, W. Wang, X. Zhou, S. Guo, Individual nanocomposite sheets of chemically reduced graphene oxide and poly (N-vinyl pyrrolidone): preparation and humidity sensing characteristics, J. Mater. Chem., 20 (2010) 10824-10828.

[38] T. Lin, I.-W. Chen, F. Liu, C. Yang, H. Bi, F. Xu, F. Huang, Nitrogen-doped mesoporous carbon of extraordinary capacitance for electrochemical energy storage, Science, 350 (2015) 1508-1513.
[39] B. Kaur, T. Pandiyan, B. Satpati, R. Srivastava, Simultaneous and sensitive determination of ascorbic acid, dopamine, uric acid, and tryptophan with silver nanoparticles-decorated reduced graphene oxide modified electrode, Colloids Surf. B. Biointerfaces, 111 (2013) 97-106.
[40] M. Ionita, A.M. Pandele, L. Crica, L. Pilan, Improving the thermal and mechanical properties of polysulfone by incorporation of graphene oxide, Compos. Part B. Eng., 59 (2014) 133-139.
[41] R. Xu, C. Wu, H. Xu, Particle size and zeta potential of carbon black in liquid media, Carbon, 45 (2007) 2806-2809.
[42] B. Wei, B. Zhang, B. Sun, Z. Jin, X. Xu, Y. Tian, Aqueous re-dispersibility of starch nanocrystal powder improved by sodium hypochlorite oxidation, Food Hydrocolloids, 52 (2016) 29-37.
[43] R. Müller, C. Jacobs, Buparvaquone mucoadhesive nanosuspension: preparation, optimisation and long-term stability, Int. J. Pharm., 237 (2002) 151-161.
[44] L. He, L.F. Dumée, C. Feng, L. Velleman, R. Reis, F. She, W. Gao, L. Kong, Promoted water transport across graphene oxide–poly(amide) thin film composite membranes and their antibacterial activity, Desalination, 365 (2015) 126-135.
[45] R. Ding, H. Zhang, Y. Li, J. Wang, B. Shi, H. Mao, J. Dang, J. Liu, Graphene oxide-embedded nanocomposite membrane for solvent resistant nanofiltration with enhanced rejection ability, Chem. Eng. Sci., 138 (2015) 227-238.
[46] H.-R. Chae, J. Lee, C.-H. Lee, I.-C. Kim, P.-K. Park, Graphene oxide-embedded thin-film composite reverse osmosis membrane with high flux, anti-biofouling, and chlorine resistance, J. Membr. Sci., 483 (2015) 128-135.
[47] Y. Song, P. Sun, L. Henry, B. Sun, Mechanisms of structure and performance controlled thin film composite membrane formation via interfacial polymerization process, J. Membr. Sci., 251 (2005) 67-79.
[48] S.-T. Yang, Y. Chang, H. Wang, G. Liu, S. Chen, Y. Wang, Y. Liu, A. Cao, Folding/aggregation of graphene oxide and its application in Cu 2+ removal, J. Colloid Interface Sci., 351 (2010) 122-127.
[49] H.-R. Chae, C.-H. Lee, P.-K. Park, I.-C. Kim, J.-H. Kim, Synergetic effect of graphene oxide nanosheets embedded in the active and support layers on the performance of thin-film composite membranes, J. Membr. Sci., (2016).
[50] S. Xia, L. Yao, Y. Zhao, N. Li, Y. Zheng, Preparation of graphene oxide modified polyamide thin film composite membranes with improved hydrophilicity for natural organic matter removal, Chem. Eng. J., 280 (2015) 720-727.
[51] X. Liu, Y. Xu, Z. Wu, H. Chen, Poly (N‐vinylpyrrolidone)‐Modified Surfaces for Biomedical Applications, Macromol. Biosci., 13 (2013) 147-154.
[52] Q. She, R. Wang, A.G. Fane, C.Y. Tang, Membrane fouling in osmotically driven membrane processes: a review, J. Membr. Sci., 499 (2016) 201-233.
[53] S. Qi, Y. Li, R. Wang, C.Y. Tang, Towards improved separation performance using porous FO membranes: The critical roles of membrane separation properties and draw solution, J. Membr. Sci., 498 (2016) 67-74.